vehicles

MDPI

Article

Research on Semi-Active Suspension Attitude Control for Commercial Vehicle Cab Under Braking and Steering Conditions

Yang Jin [1], Zhanyun An [1], Liang Li [2], Jun Liu [3], Yiyang Liu [1] and Changcheng Yin [1,*]

[1] School of Automotive Engineering, Hubei University of Automotive Technology, Shiyan 442002, China; jiny_qc@huat.edu.cn (Y.J.); 202411302@huat.edu.cn (Z.A.); 202311024@huat.edu.cn (Y.L.)
[2] Engineering Validation Center, Product R&D Institute, Dongfeng Motor Co., Ltd., Wuhan 430000, China; gf-liliang1@dfac.com
[3] Product Service Center, Xiangyang DAAN Automobile Test Center Co., Ltd., Xiangyang 441000, China; liujun@nast.com.cn
* Correspondence: changchengy_huat@163.com

Abstract

During transient maneuvers such as emergency braking and steering, the cab attitude of a commercial vehicle may change abruptly, thereby posing a potential risk to driving safety. To address this issue, this study investigates a cab attitude control method for a specific commercial vehicle under braking and steering conditions based on a semi-active suspension system. First, full-vehicle road tests were conducted under emergency braking and steering conditions. The measured signals at the lower mounting points of the cab suspension were collected, preprocessed, and used as disturbance inputs to the system. Subsequently, performance tests were carried out on a continuous damping control (CDC) damper, and forward and inverse interpolation-based lookup table models of the damper, together with a three-degree-of-freedom predictive model of the cab, were established. In addition, a model predictive control (MPC) controller for the semi-active suspension was designed based on the predictive model, with different performance indices formulated for the braking and steering conditions. Finally, the control effectiveness of the MPC method on the cab attitude responses under braking and steering conditions was evaluated using the MATLAB/Simulink platform. The results show that the proposed control method can effectively improve the dynamic responses of the cab in terms of vertical acceleration, pitch angular acceleration, and roll angular acceleration, thereby mitigating braking- and steering-induced cab attitude deviations.

Keywords: cab semi-active suspension; model predictive control; dynamic model; adjustable damping shock absorber; evaluation index

Check for updates

Academic Editor: Oluremi Ayotunde Olatunbosun

Received: 14 August 2026
Revised: 17 September 2026
Accepted: 23 September 2026
Published: 24 September 2026

Copyright: © 2026 by the authors. Licensee MDPI, Basel, Switzerland. This article is an open access article distributed under the terms and conditions of the Creative Commons Attribution (CC BY) license.

1. Introduction

Commercial vehicles, serving as the primary transportation means for road freight and engineering operations, are continuously subjected to high-intensity and long-duration transportation tasks. Cab vertical vibration and pitch/roll motion directly affect driver ride comfort, fatigue, and driving safety, making it one of the key indicators for evaluating the comprehensive performance of commercial vehicles. Compared with passenger vehicles, commercial vehicles exhibit distinct characteristics, including larger curb mass and a higher center of gravity, which make them more prone to complex coupled vibrations and attitude deviations under both normal driving conditions and transient maneuvers. In particular, typical transient conditions such as emergency braking and steering can induce

dynamic responses significantly different from those caused by random road excitation. These responses have become major factors contributing to cab vibration deterioration and attitude instability [1], thereby seriously affecting ride comfort, driving safety, and vehicle stability. Due to the fixed damping and stiffness parameters, conventional passive suspensions cannot adaptively adjust their characteristics according to dynamic driving conditions, making it difficult to simultaneously satisfy the requirements of attitude stability and vibration suppression under transient maneuvers such as emergency braking and steering. Consequently, passive suspensions exhibit significant limitations in adapting to diverse operating conditions [2].

In recent years, active suspension systems have also been extensively investigated for commercial and heavy-duty vehicles. Metered and Ibrahim [3] employed active suspension control to improve the ride comfort and road friendliness of a commercial vehicle equipped with a tandem axle suspension. Gong et al. [4] developed an active suspension strategy for a heavy rescue vehicle based on multi-sensor information fusion, demonstrating improvements in vertical, pitch, and roll responses. Xu et al. [5] investigated coordinated road-tracking and anti-roll control for commercial vehicles to improve roll stability under steering-related conditions. Pang et al. [6] proposed a preview-based MPC strategy for heavy-duty vehicle active suspension to coordinate ride comfort and roll stability, while Ma et al. [7] combined online vehicle mass estimation with active suspension control for trucks to improve the robustness of suspension performance under varying load conditions. Do [8] developed a constrained MPC strategy for an in-wheel active suspension system, in which system constraints were explicitly incorporated into the optimization problem to improve ride comfort and road-holding performance. These studies demonstrate the effectiveness of active suspension systems in multi-objective vibration and attitude regulation of commercial vehicles.

Active suspension methods can provide a broader control force range and have been combined with LQR, MPC, and optimization algorithms to improve ride and attitude performance. However, their higher energy demand and actuator requirements limit direct application to commercial-vehicle cab suspensions. Semi-active suspensions offer a compromise between control authority, energy consumption, and engineering feasibility. Recent studies have therefore investigated intelligent, optimization-based, and predictive semi-active control strategies. Benefiting from adjustable parameters, rapid response capability, low energy consumption, and high reliability, semi-active suspensions have gradually become a mainstream solution for cab vibration and attitude control in commercial vehicles.

Existing studies have primarily focused on vertical vibration optimization under conventional random road excitations [9]. Although extensive investigations have been conducted on the control of steady-state pitch vibrations induced by impact road surfaces, the excitation inputs of vehicle models are generally generated using filtered white noise methods rather than obtained from actual road tests of real vehicles [10,11]. Moreover, existing studies have predominantly focused on whole-vehicle suspension responses under road excitation, whereas the coordinated control of commercial-vehicle cab pitch and roll responses under measured transient braking and steering disturbances remains comparatively less explored. Therefore, the engineering applicability of these studies remains limited.

Furthermore, targeted control strategies for suppressing cab pitch and roll motions under typical transient maneuvers, such as emergency braking and steering, have received relatively insufficient attention. During emergency braking, the longitudinal impact force can intensify cab pitch motion, resulting in vehicle nose-diving and visual field disturbances [12–14]. During steering maneuvers, centrifugal loads tend to induce cab roll deviations, thereby deteriorating the balance of vehicle attitude stability [15–17]. Therefore,

the specific pitch- and roll-response issues associated with these two typical transient conditions need to be effectively addressed through specially designed control strategies.

Based on the above studies, active and semi-active suspension control has demonstrated considerable potential for improving vehicle ride comfort and attitude responses. However, several issues remain insufficiently addressed for commercial-vehicle cab attitude control under transient maneuvers. First, many existing studies employ numerically generated road excitations, whereas the actual disturbances transmitted from the chassis to the cab during emergency braking and steering have received comparatively limited attention. Second, the nonlinear characteristics and physical operating constraints of practical controllable dampers are not always explicitly considered in control-oriented suspension models. Third, braking- and steering-induced attitude motions exhibit different dominant characteristics, with pitch being more critical during braking and roll being more pronounced during steering. Therefore, a condition-oriented semi-active suspension control strategy capable of coordinating vertical, pitch, and roll responses under experimentally measured transient disturbances is still required.

Compared with recent MPC-based active suspension studies, the present study addresses a different control problem and implementation framework. Rather than focusing primarily on vertical vibration and road-holding performance under numerically generated road excitations, the proposed method targets the coordinated vertical, pitch, and roll responses of a commercial-vehicle cab under measured transient braking and steering disturbances. The distinguishing feature of the proposed framework lies not in the MPC algorithm itself, but in the integration of real-vehicle measured disturbances, experimentally characterized nonlinear CDC damper behavior, and condition-dependent coordinated control of the four controllable damper forces.

On this basis, the specific contributions of the present study are summarized as follows: (1) real-vehicle road tests are conducted under emergency-braking and right-angle-steering conditions, and the measured vibration signals at the four lower cab-suspension mounting points are processed and employed as disturbance inputs, thereby preserving the excitation characteristics actually transmitted from the chassis to the cab; (2) the nonlinear force–velocity–current characteristics of the front and rear CDC dampers are obtained experimentally, and forward and inverse interpolation-based lookup table models are established to determine the actual damper forces and corresponding control currents in the semi-active control loop; and (3) a three-degree-of-freedom control-oriented prediction model incorporating the vertical, pitch, and roll motions of the cab is established, based on which an MPC strategy with condition-dependent weighting is developed to coordinate the four controllable damper forces. Greater emphasis is placed on pitch suppression during braking and roll suppression during steering while the vertical response is simultaneously included in the optimization objective, thereby enabling coordinated cab attitude control under the two investigated transient operating conditions.

2. Real-Vehicle Road Sampling Test

To acquire the dynamic response characteristics of the cab suspension system under typical emergency braking and steering conditions, real-vehicle road sampling tests were performed on a commercial truck. The measured vibration signals were subsequently utilized as excitation inputs for the vehicle dynamics model and control algorithm simulations. The vehicle schematic is shown in Figure 1. Prior to testing, the suspension components and articulation joints of the vehicle were systematically inspected to verify the integrity of mechanical connections and ensure that the vibration isolation performance of the suspension system remained within normal operating conditions.



Figure 1. Test vehicle.

2.1. Test Conditions and Experimental Scheme

The road test environment and general measurement procedures were established with reference to GB/T 4970-2009 [18], "Method of Running Test—Automotive Ride Comfort," a Chinese national standard applicable to M- and N-category vehicles for ride comfort testing under pulse and random road inputs. It should be noted that the standard was used in the present study as a reference for general test conditions and measurement practice rather than to define the emergency-braking and right-angle-steering maneuvers themselves.

Specifically, GB/T 4970-2009 specifies a dry test road with a longitudinal gradient not exceeding 1%, a wind speed not exceeding 5 m/s, appropriate vehicle technical conditions, and stable and reliable vibration measurement equipment.

The road tests were conducted on a closed test track within Hubei University of Automotive Technology. The road surface conditions satisfied the flatness requirements specified in GB/T 4970-2009, "Method of Road Test for Evaluating Ride Comfort of Automobiles", with a longitudinal gradient of less than 1%. The road surface was dry, providing suitable conditions for emergency braking tests. Meanwhile, a right-angle curve at an intersection of the campus road was selected for steering maneuver tests. The curve radius was approximately 12 m, representing a typical right-angle steering condition encountered in urban roads and conventional highways. The ambient temperature during the tests was approximately 30 °C, with a wind speed of Beaufort scale 2–3. During all experiments, the vehicle cabin remained in an unladen condition. Only one driver and one test engineer were present inside the cab, with a combined occupant mass of approximately 150 kg. According to the recommendations of ISO 2631-1:1997 [19], the occupants were required to maintain a standard sitting posture and fasten seat belts during the tests to minimize the influence of human biodynamic responses on the measurement results. The measurement system consisted of PCB 356A16 tri-axial accelerometers and an LMS SCADAS data acquisition system.

Prior to testing, the sensitivity coefficients of the X-, Y-, and Z-direction channels were individually configured in Simcenter Testlab according to the calibration certificates of each accelerometer.

To obtain the vibration excitation inputs at the lower mounting points of the cab suspension system, tri-axial accelerometers were installed on the active sides of the four cab suspensions (front-left, front-right, rear-left, and rear-right), i.e., the connection points between the suspensions and the vehicle frame. The acceleration signals in the longitudinal (X), lateral (Y), and vertical (Z) directions were simultaneously measured, and the sensor arrangement is illustrated in Figure 2.



(**a**) Front-left suspension mount lower end.



(**b**) Front-right suspension mount lower end.



(**c**) Rear-left suspension mount lower end.



(**d**) Rear-right suspension mount lower end.

Figure 2. Acceleration sensor layout.

To establish a consistent reference coordinate system for subsequent data processing and analysis, a vehicle coordinate system was defined as follows: the forward direction of the vehicle was defined as the positive *X*-axis, the driver's left-hand direction as the positive *Y*-axis, and the upward vertical direction as the positive *Z*-axis. The channel direction mapping in Simcenter Testlab was configured according to this coordinate definition.

Because the purpose of the present experiment was to obtain the actual disturbance inputs transmitted from the vehicle frame to the cab suspension rather than to perform a

conventional occupant ride-comfort assessment, the accelerometers were installed at the four lower cab-suspension mounting points instead of the occupant-interface locations prescribed for conventional ride-comfort measurements in GB/T 4970-2009. The maneuver speeds and loading condition were also selected specifically for the investigated transient braking and steering scenarios.

For the emergency braking maneuver, the initial test speed was set to 20 km/h. The vehicle was accelerated to the target speed and maintained at a constant velocity for at least 20 m to achieve a stable dynamic state. Subsequently, the driver performed emergency braking until the vehicle came to a complete stop. Data acquisition was triggered before the onset of braking operation, with a recording duration of 10 s and a sampling frequency of 100 Hz. For the right-angle steering maneuver, the entry speed was set to 25 km/h. Before testing, a turning reference marker was placed at the entrance of the right-angle curve to ensure consistent steering initiation positions. During the test, the vehicle accelerated to 25 km/h on the straight section and maintained a constant speed. When reaching the designated marker, the driver initiated the steering maneuver and passed through the right-angle curve with a constant steering wheel angle. After exiting the curve, the vehicle continued traveling in a straight line for a certain distance. Data acquisition was triggered approximately 2 s before entering the curve, with each recording lasting 10 s at a sampling frequency of 100 Hz, covering the complete process of curve entry, turning, and steering recovery.

For both test conditions, the effective signal duration was determined as 5 s after observation and extraction of the measured vibration responses. This duration was sufficient to preserve the dominant vibration characteristics induced by the corresponding transient maneuvers.

2.2. Experimental Results and Signal Processing

According to the aforementioned test procedures, the time-domain acceleration signals in the vertical direction (Z-direction) at the lower mounting points of the four cab suspensions were collected under the emergency braking condition at 20 km/h and the right-angle steering condition at 25 km/h. To provide a more complete description of the measured disturbances used in this study, Figure 3 presents the original acceleration response curves measured at the lower mounting points of the cab suspensions under both the emergency-braking and right-angle-steering conditions.

After obtaining the acceleration signals under the two transient operating conditions, the displacement signals were obtained through two successive numerical integrations and were subsequently used as input excitations for the simulation model. The raw acceleration signals measured during the road tests inevitably contained high-frequency components, minor measurement errors, and sensor noise. If the raw acceleration signals were directly subjected to double integration, the bias and low-frequency drift would be accumulated and further amplified during the integration process, thereby reducing the reliability of the reconstructed displacement signals [20]. Therefore, filtering preprocessing was performed before acceleration integration, and trend terms were suppressed during the integration process to obtain more accurate displacement excitation inputs [21,22].

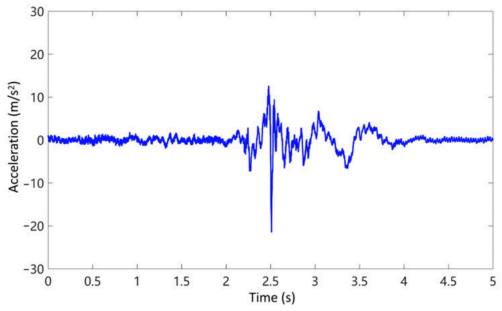

(**a**) Front-left suspension mount lower-end signal.

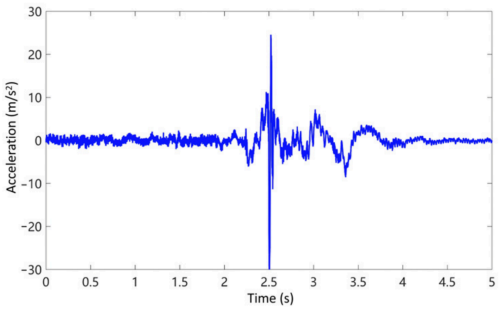

(**b**) Front-right suspension mount lower-end signal.

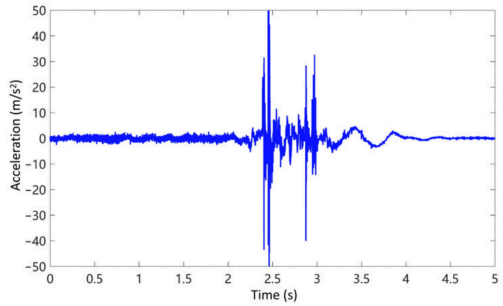

(**c**) Rear-left suspension mount lower-end signal.

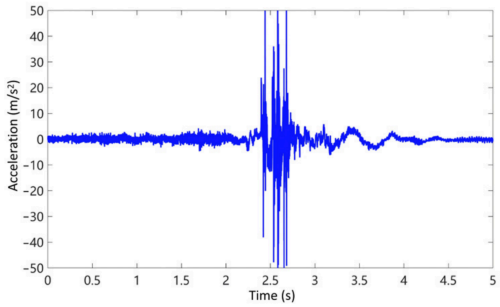

(**d**) Rear-right suspension mount lower-end signal.

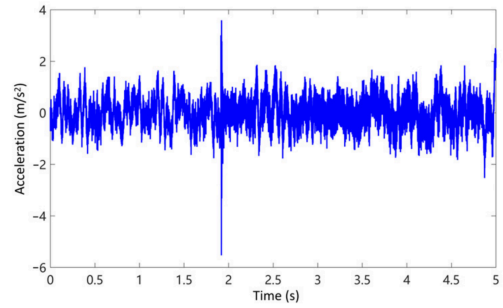

(**e**) Front-left suspension mount lower-end signal.

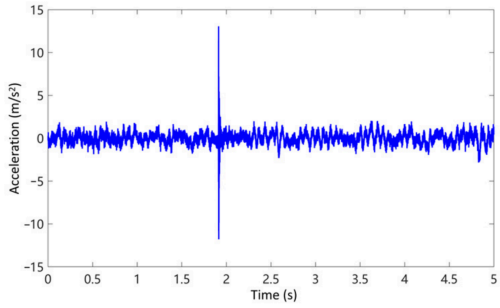

(**f**) Front-right suspension mount lower-end signal.

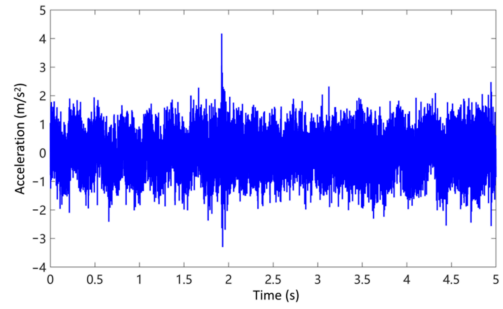

(**g**) Rear-left suspension mount lower-end signal.

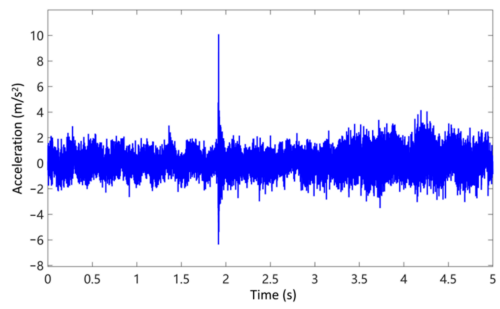

(**h**) Rear-right suspension mount lower-end signal.

Figure 3. Acceleration signals at the lower ends of the cab suspension mounts under (**a**–**d**) the 20 km/h emergency-braking condition and (**e**–**h**) the 25 km/h right-angle-steering condition.

This study primarily focuses on the vertical acceleration responses at the lower mounting points of the cab suspensions under braking and steering maneuvers. According to the frequency characteristics of the measured signals, the dominant effective components are mainly distributed within the range of 0.2–20 Hz [23]. Accordingly, a frequency band of 0.2–20 Hz was selected as the passband, and a fourth-order Butterworth band-pass filter was employed to preprocess the raw acceleration signals. To minimize the influence of phase delay on the time-domain waveforms, forward–backward zero-phase filtering based

on the filtfilt function was applied during the filtering process, thereby avoiding significant shifts in peak positions and waveform distortion [24]. Meanwhile, the filtered acceleration signals were integrated using a fourth-order Runge–Kutta discrete integration scheme [25], which effectively suppresses the interference caused by trend terms during the numerical integration process. Assuming that a_k represents the acceleration value at the k-th sampling point after zero-mean processing, and h denotes the sampling interval, the velocity can be expressed as:

$$v_k = v_{k-1} + \frac{h}{6}(k_1 + 2k_2 + 2k_3 + k_4) \quad (1)$$

where v_k denotes the velocity value corresponding to the k-th sampling point, while k_1, k_2, k_3, and k_4 are the intermediate variables defined in the fourth-order Runge–Kutta integration algorithm. Since slowly varying drift components may still exist in the velocity signal after the first integration, a sliding-window correction method was subsequently applied to further eliminate the residual trend terms. The corrected velocity expression can be formulated as follows:

$$v'_k = v_k - \frac{v_{\max} + v_{\min}}{2} \quad (2)$$

where $v_{\max}$ and $v_{\min}$ denote the maximum and minimum values of the velocity signal within the current sliding window, respectively, and the window size is selected as 100 sampling points. After the drift correction, the corrected velocity signal was integrated again following the same procedure to obtain the displacement time histories of the lower attachment points of the cab suspension. The acceleration signals measured under both operating conditions were processed using the same band-pass filtering, zero-mean, drift-correction, and double-integration procedures. Figure 4 presents the reconstructed displacement inputs under the braking condition as a representative example; the steering-condition inputs were obtained using the identical procedure and were used in the corresponding simulations.

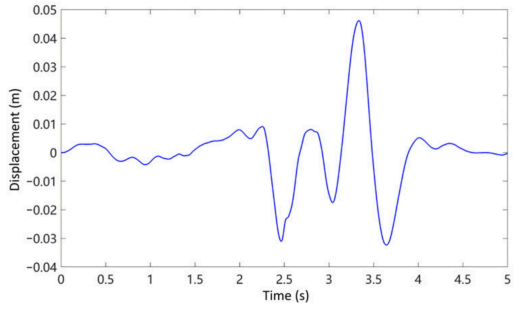

(**a**) Front-left suspension mount lower-end signal.

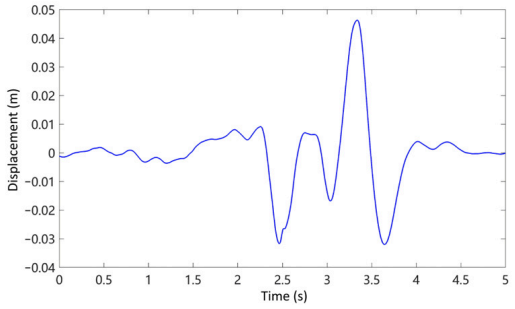

(**b**) Front-right suspension mount lower-end signal.

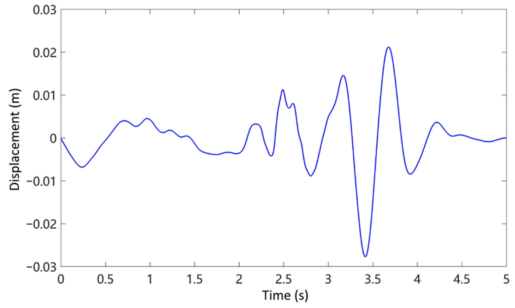

(**c**) Rear-left suspension mount lower-end signal.

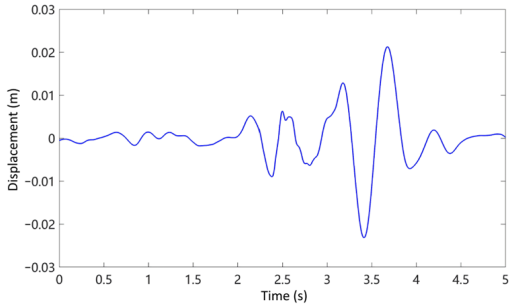

(**d**) Rear-right suspension mount lower-end signal.

Figure 4. Displacement signals at the lower ends of the cab suspension mounts under the 20 km/h emergency braking condition, presented as a representative example.

3. Development of the Cab Suspension Dynamic Model

3.1. Performance Testing and Modeling of the CDC Damper

The CDC damper is the key actuator component in a semi-active cab suspension system. Based on vehicle state information acquired by sensors, the controller determines the control current, and the CDC damper adjusts its damper force accordingly within a short response time. Consequently, the dynamic response of the cab can be modified through real-time regulation of the damping characteristics [26].

In this study, a single-solenoid-valve CDC damper adapted for the front and rear cab suspension systems of the target commercial vehicle was selected as the test specimen. The performance tests were conducted in accordance with the requirements specified in QC/T 491-2018, "Performance Requirements and Bench Test Methods for Automotive Shock Absorbers" [27]. The primary objective of the test was to obtain the three-dimensional relationship among damper force, piston velocity, and control current of the single-solenoid-valve CDC damper through a damper dynamometer test. The experimental setup used in the test is shown in Figure 5.

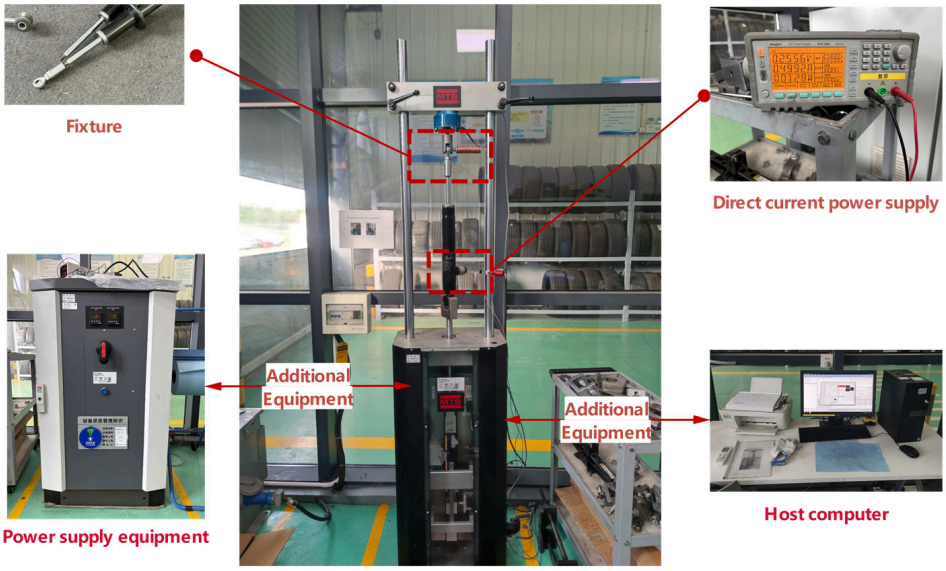

Figure 5. Test equipment for the CDC damper.

During the test, the CDC damper was vertically fixed on the test bench using a dedicated fixture, and its external solenoid valve was independently powered by an external DC regulated power supply. The test amplitude of the damper was set to ±25 mm. The control current range was 0.3–1.9 A, with an increment of 0.2 A. Eight characteristic velocity inputs within the range of 0.052–0.918 m/s were selected. The external characteristic test conditions of the damper were constructed by combining nine different current inputs and eight different velocity rates to investigate the effects of current and velocity on the damper force.

After completion of the tests, the measured data were processed and analyzed. The multi-condition mechanical characteristics of the tested damper were determined based on the damper force–displacement characteristics and velocity characteristics. Figure 6 presents the force–displacement characteristic curves of the CDC dampers used in the front and rear suspensions under two current inputs of 0.5 A and 1.1 A. Figure 7 shows the velocity characteristic curves of the CDC dampers for the front and rear suspensions under different current inputs.

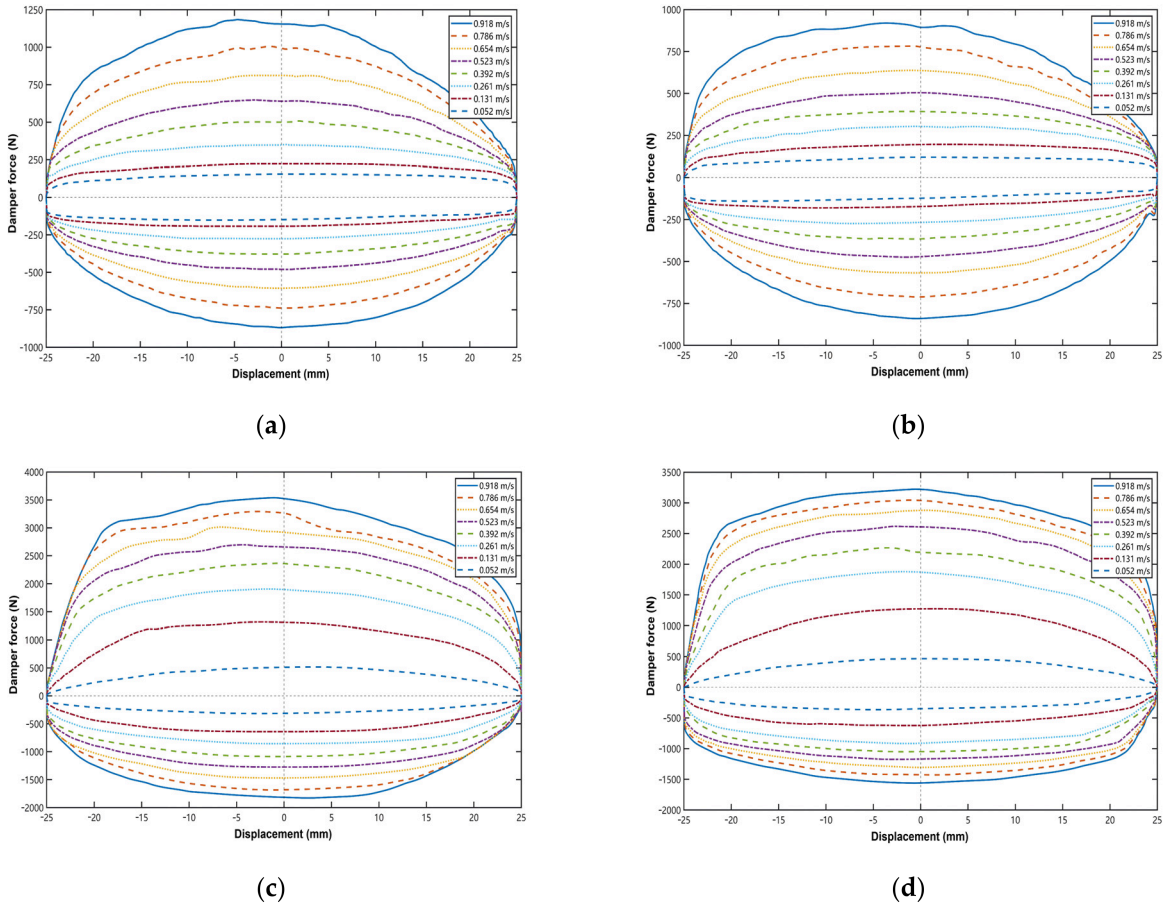

Figure 6. Force–displacement hysteresis curves of the front and rear CDC dampers. (**a**) Force–displacement hysteresis curve of the front CDC damper at 0.5 A. (**b**) Force–displacement hysteresis curve of the rear CDC damper at 0.5 A. (**c**) Force–displacement hysteresis curve of the front CDC damper at 1.1 A. (**d**) Force–displacement hysteresis curve of the rear CDC damper at 1.1 A.

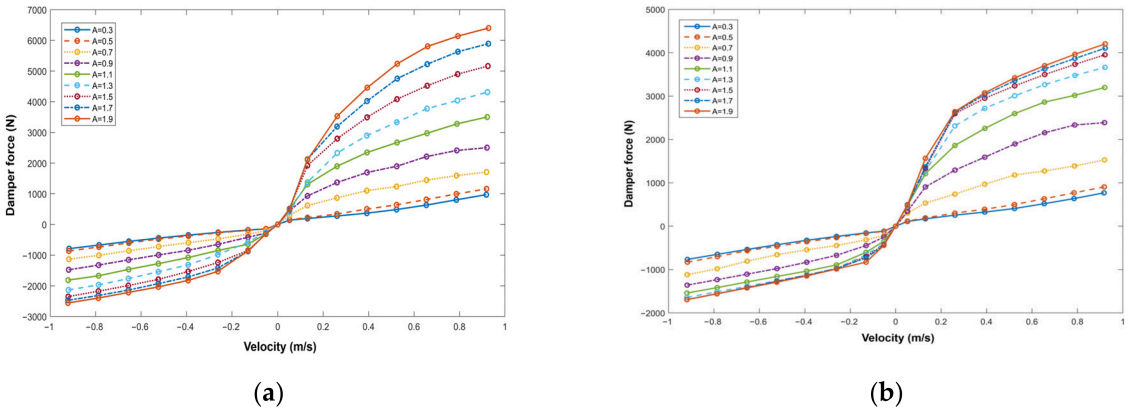

Figure 7. Velocity characteristic curves of the front and rear CDC dampers. (**a**) Velocity characteristic curves of the front CDC damper under different current inputs. (**b**) Velocity characteristic curves of the rear CDC damper under different current inputs.

Within the low current range (0.3–0.5 A), the characteristic curves of the front and rear dampers are relatively close. In this range, the throttling effect of the solenoid valve is weak, resulting in a small variation in damper force. When the input current increases, the damper force of the damper increases accordingly, and a certain degree of saturation phenomenon occurs at higher current levels. The velocity characteristic curves can be used to determine the adjustable range of the damper force and its nonlinear relationship, which

is beneficial for the subsequent selection of the damper modeling method and the design of the control algorithm.

In recent years, the application of neural networks in damper modeling has attracted extensive attention [28,29]. By using neural networks to perform nonlinear fitting of experimental data, the data continuity and noise resistance of CDC damper models can be effectively improved, thereby enhancing the numerical solution stability of nonlinear prediction models. However, neural network models usually involve a large number of multiply–add operations and activation function calculations. During simulation and controller hardware deployment, they require considerable computational resources, significantly reducing the available online optimization solution time of control algorithms. Therefore, they are difficult to satisfy the requirements of real-time control.

To balance the nonlinear representation capability of the CDC damper model and the real-time performance of the control strategy, an interpolation lookup table method is adopted to establish the damper model in this study. Based on the damper force data obtained from the aforementioned performance tests under different input currents and motion velocities, as well as the nonlinear mapping relationship among these variables, a forward lookup table model of the CDC damper is constructed. The model takes the input current and damper motion velocity as inputs and the damper force as the output. The three-dimensional surface of the damper force varying with the input current and motion velocity obtained through interpolation calculation is shown in Figure 8.

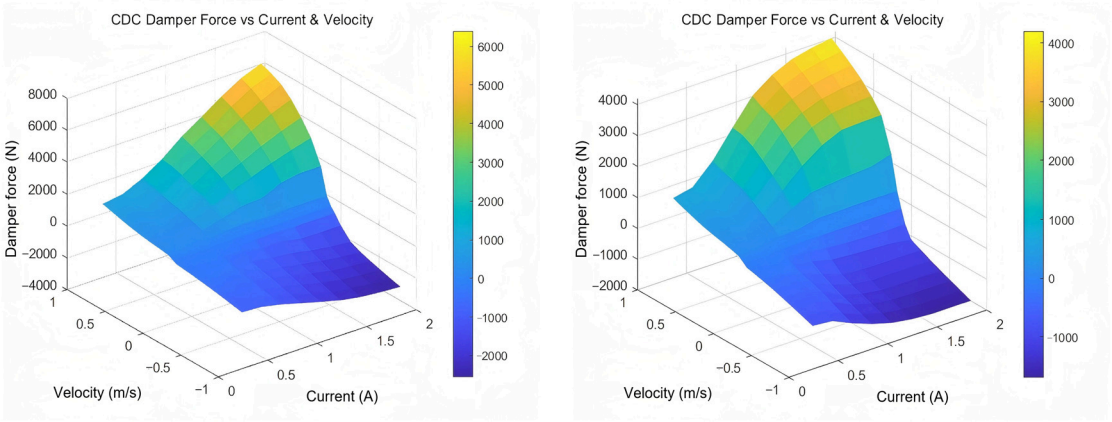

(**a**) (**b**)

Figure 8. Interpolated three-dimensional maps of the damper force–current–velocity relationship for the front and rear CDC dampers. (**a**) Interpolation surface of the force–current–velocity relationship for the front CDC damper. (**b**) Interpolation surface of the force–current–velocity relationship for the rear CDC damper.

Based on the forward lookup table model, an inverse model is constructed from the nonlinear relationship among damper force, control current, and damper velocity. During closed-loop simulation, the MPC controller first computes the desired controllable damper force from the cab motion state. The inverse model then determines the corresponding control current using the instantaneous damper velocity, and the forward model calculates the actual damper force. This actual damper force is supplied to the cab-suspension dynamic model, completing the semi-active control loop.

3.2. Cab Suspension Dynamic Model

The cab, considered as the controlled object in this study, can be described by three degrees of freedom, including vertical translational motion, pitch rotational motion, and roll rotational motion. In this study, the cab suspension system of a certain type of commercial

vehicle was simplified, and the mass of the cab and related components was equivalently concentrated at the center of gravity of the cab. A three-degree-of-freedom cab suspension dynamic model was established. Meanwhile, the vertical displacement of the lower ends of the cab suspensions was considered as the known disturbance input of the system. The schematic diagram of the established cab suspension dynamic model is shown in Figure 9.

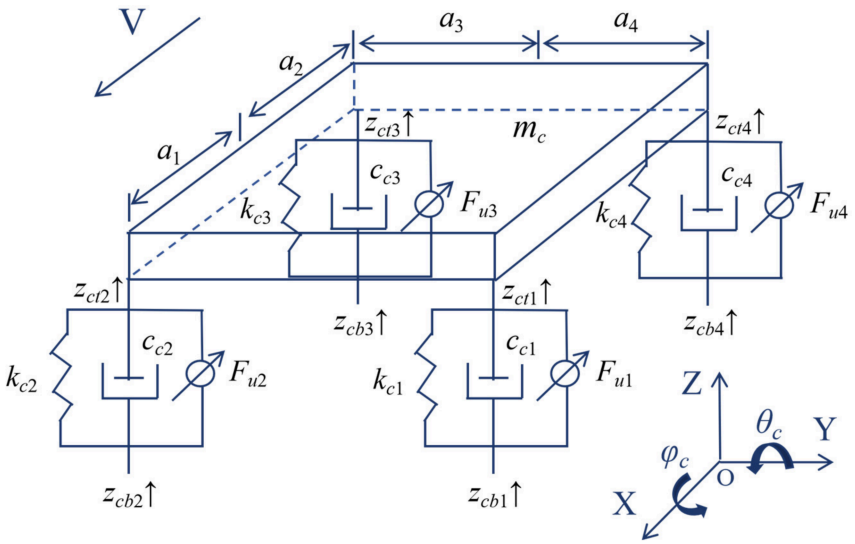

Figure 9. Schematic diagram of the three-degree-of-freedom cab suspension model.

The dynamic equation of the cab suspension system is given as follows:

$$\begin{aligned}
m_c\ddot{z}_c &= \sum_{i=1}^{4}\left[k_{ci}(z_{cbi}-z_{cti})+c_{ci}(\dot{z}_{cbi}-\dot{z}_{cti})+F_{ui}\right]\\
I_{c\theta}\ddot{\theta}_c &= \sum_{i=3}^{4}\left[k_{ci}(z_{cbi}-z_{cti})+c_{ci}(\dot{z}_{cbi}-\dot{z}_{cti})+F_{ui}\right]a_2\\
&\quad-\sum_{i=1}^{2}\left[k_{ci}(z_{cbi}-z_{cti})+c_{ci}(\dot{z}_{cbi}-\dot{z}_{cti})+F_{ui}\right]a_1\\
I_{c\varphi}\ddot{\varphi}_c &= \left[k_{c1}(z_{cb1}-z_{ct1})+c_{c1}(\dot{z}_{cb1}-\dot{z}_{ct1})+F_{u1}\right.\\
&\quad\left.+k_{c3}(z_{cb3}-z_{ct3})+c_{c3}(\dot{z}_{cb3}-\dot{z}_{ct3})+F_{u3}\right]a_4\\
&\quad-\left[k_{c2}(z_{cb2}-z_{ct2})+c_{c2}(\dot{z}_{cb2}-\dot{z}_{ct2})+F_{u2}\right.\\
&\quad\left.+k_{c4}(z_{cb4}-z_{ct4})+c_{c4}(\dot{z}_{cb4}-\dot{z}_{ct4})+F_{u4}\right]a_3
\end{aligned} \tag{3}$$

For the braking and steering conditions investigated in this study, the cab pitch and roll motions are considered to remain within a relatively small angular range. Accordingly, a small-angle approximation is adopted in establishing the control-oriented cab model, i.e., $\sin\theta_c \approx \theta_c$, $\sin\varphi_c \approx \varphi_c$, and $\cos\theta_c \approx \cos\varphi_c \approx 1$. Based on this assumption, the vertical displacements of the four upper suspension mounting points can be approximated as linear combinations of the vertical displacement, pitch angle, and roll angle of the cab center of gravity, as expressed in Equation (4).

$$\begin{cases}
z_{ct1} = z_c - a_1\theta_c + a_4\varphi_c\\
z_{ct2} = z_c - a_1\theta_c - a_3\varphi_c\\
z_{ct3} = z_c + a_2\theta_c + a_4\varphi_c\\
z_{ct4} = z_c + a_2\theta_c - a_3\varphi_c
\end{cases} \tag{4}$$

where m_c represents the mass of the cab, and $I_{c\theta}$ and $I_{c\varphi}$ represent the moments of inertia of the cab about the Y-axis and X-axis, respectively. z_c, θ_c, and φ_c denote the vertical displacement, pitch angle, and roll angle of the cab center of gravity, respectively. z_{cbi} and

$z_{ct\mathrm{i}}$ represent the vertical displacements of the lower and upper mounting points of the i-th suspension, respectively. $F_{u\mathrm{i}}$ is the controllable damper force at the i-th cab suspension, where i = 1,2,3,4. $k_{c\mathrm{i}}$ and $c_{c\mathrm{i}}$ represent the suspension stiffness and damping coefficient of the i-th suspension, respectively. a_1, a_2, a_3, and a_4 denote the distances from the front/rear and left/right suspension mounting points to the cab center of gravity, respectively. The numerical values of the model parameters are listed in Table 1.

Table 1. Parameters of the Cab Suspension Model.

Parameter Name	Symbol	Value	Unit
Cab mass	m_c	980	kg
Moment of inertia of the cab about the Y-axis	$I_{c\theta}$	2264	kg·m^2
Moment of inertia of the cab about the X-axis	$I_{c\varphi}$	346	kg·m^2
Front cab suspension stiffness	k_{c1}, k_{c2}	45,000	N/m
Rear cab suspension stiffness	k_{c3}, k_{c4}	35,000	N/m
Intrinsic damping coefficient of the CDC damper in the front suspension	c_{c1}, c_{c2}	929	N·s/m
Intrinsic damping coefficient of the CDC dampers in the rear suspension	c_{c3}, c_{c4}	798	N·s/m
Longitudinal distance from the front suspension to the cab center of gravity	a_1	0.7	m
Longitudinal distance from the rear suspension to the cab center of gravity	a_2	0.8	m
Half of the lateral distance between the left and right suspensions	a_3, a_4	0.6	m

The three-degree-of-freedom semi-active cab suspension dynamic model is adopted in this study, mainly based on the following reasons:

(1) The vibration displacement at the lower mounting points of the suspensions can be directly obtained through road tests, and these signals already contain the transmission and filtering characteristics of the chassis suspension system with respect to road excitations. Therefore, it is unnecessary to establish complex tire–road and chassis suspension models. This reduces the model complexity, weakens the dependence of the controller on the accuracy of the full vehicle model, and improves the engineering applicability of the control method.

(2) The cab suspension control acts between the cab and the vehicle frame, and its control performance mainly depends on the relative motion state between the upper and lower ends of the suspensions. By considering the displacement of the suspension lower ends as a known disturbance, a prediction model can be established with the desired controllable damper force as the control input and the cab motion state as the output, providing the foundation for subsequent controller design.

By substituting Equation (4) into Equation (3) and arranging the equations into matrix form, the three-degree-of-freedom dynamic equation of the cab can be obtained as follows:

$$M_c\ddot{q}_c + C_c\dot{q}_c + K_c q_c = B_u u + B_d d + C_d\dot{d} \tag{5}$$

where $q_c = [z_c, \theta_c, \varphi_c]^{\mathrm{T}}$ is the cab state vector, $u = [F_{u1}, F_{u2}, F_{u3}, F_{u4}]^{\mathrm{T}}$ is the desired controllable damper force vector, and $d = [z_{cb1}, z_{cb2}, z_{cb3}, z_{cb4}]^{\mathrm{T}}$ is the displacement vector of the lower mounting points of the suspensions. $z_{ct} = [z_{ct1}, z_{ct2}, z_{ct3}, z_{ct4}]^{\mathrm{T}}$ is the displacement vector of the upper mounting points of the suspensions, and it satisfies $z_{ct} = \mathrm{H}q_c$,

where H is the geometric transformation matrix $\mathrm{H} = \begin{bmatrix} 1 & -a_1 & a_4 \\ 1 & -a_1 & -a_3 \\ 1 & a_2 & a_4 \\ 1 & a_2 & -a_3 \end{bmatrix}$. The stiffness and damping diagonal matrices of the suspensions are defined as $K_s = \mathrm{diag}(k_{c1}, k_{c2}, k_{c3}, k_{c4})$, $C_s = \mathrm{diag}(c_{c1}, c_{c2}, c_{c3}, c_{c4})$. $M_c = \begin{bmatrix} m_c & 0 & 0 \\ 0 & I_{c\theta} & 0 \\ 0 & 0 & I_{c\varphi} \end{bmatrix}$, $C_c = \mathrm{H}^{\mathrm{T}} C_s \mathrm{H}$, and $K_c = \mathrm{H}^{\mathrm{T}} K_s \mathrm{H}$ represent the mass, damping, and stiffness matrices, respectively. $B_u = \mathrm{H}^{\mathrm{T}}$, $B_d = \mathrm{H}^{\mathrm{T}} K_s$, and $C_d = \mathrm{H}^{\mathrm{T}} C_s$ represent the coefficient matrices corresponding to the control input, disturbance, and disturbance velocity, respectively.

Defining the state vector as $x = \left[q_c^{\mathrm{T}}, \dot{q}_c^{\mathrm{T}}\right]^{\mathrm{T}} \in \mathrm{R}^6$, Equation (3) can be expressed in the continuous-time state-space form as follows:

$$\dot{x} = A_c x + B_{u,c} u + B_{d,c} \tilde{d} \tag{6}$$

where $\tilde{d} = \left[d^{\mathrm{T}}, \dot{d}^{\mathrm{T}}\right]^{\mathrm{T}}$ is the augmented disturbance vector, $A_c = \begin{bmatrix} 0_{3\times3} & I_{3\times3} \\ -M_c^{-1}K_c & -M_c^{-1}C_c \end{bmatrix}$, $B_{u,c} = \begin{bmatrix} 0_{3\times4} \\ M_c^{-1}B_u \end{bmatrix}$, and $B_{d,c} = \begin{bmatrix} 0_{3\times4} & 0_{3\times4} \\ M_c^{-1}B_d & M_c^{-1}C_d \end{bmatrix}$. Since the displacement of the lower mounting points of the suspensions can be obtained from the measured signals, its derivative can be approximated by numerical differentiation. Therefore, the disturbance term can be regarded as a known quantity during the prediction process.

4. Design and Development of the Model Predictive Control (MPC) Controller

4.1. MPC Theory for the Cab Suspension System

Model Predictive Control (MPC) has been widely applied in the field of vehicle dynamics control due to its advantages in explicitly handling multivariable coupling, system constraints, and future dynamic prediction [30,31]. In this study, a three-degree-of-freedom linear prediction model of the cab suspension system is established for a commercial vehicle cab suspension system, and the corresponding MPC controller is designed. The prediction model takes the vertical displacement of the suspension lower mounting points as the known disturbance input and the vertical, pitch, and roll responses of the cab as the control objectives. By adjusting the four controllable damper forces, coordinated control of the cab attitude responses is achieved.

It should be noted that the linearization is introduced primarily in the control-oriented prediction model rather than in the representation of the CDC damper characteristics. Practical CDC dampers exhibit an evident nonlinear relationship among damper force, piston velocity, and control current. Therefore, in the present study, the experimentally measured nonlinear force–velocity–current characteristics are retained using forward and inverse interpolation-based lookup tables. During closed-loop simulation, the MPC controller determines the desired controllable damper force based on the linear prediction model, whereas the corresponding control current and actual damper force are subsequently determined through the nonlinear inverse and forward damper models, respectively. In this way, the linear prediction model reduces the computational complexity of online optimization, while the experimentally identified nonlinear characteristics of the actuator are retained in the closed-loop control system.

The use of a linear control-oriented model for predictive suspension control under transient vehicle maneuvers is also supported by previous studies. Zhang et al. established

a linear time-invariant half-vehicle model incorporating braking intensity and employed it as the prediction model for MPC-based active suspension control under braking conditions [32]. For steering-related maneuvers, Hegedűs et al. formulated the vertical and roll dynamics in state-space form and used the additional semi-active suspension forces as the MPC inputs, with the controller subsequently evaluated using a high-fidelity CarMaker model during lane-change maneuvers [33]. More recently, Xu et al. transformed a roll–vertical coupled vehicle model into a control-oriented linear prediction model using small-angle assumptions and demonstrated effective MPC-based roll control under double-lane-change and sinusoidal-steering conditions [34]. These studies indicate that a linear control-oriented model can provide an appropriate compromise between prediction accuracy and online computational efficiency when the vehicle operates within a moderate attitude range and the prediction horizon is relatively short.

4.2. Design of the Model Predictive Controller

Based on the aforementioned state-space model and the CDC damper performance test data, a discrete-time MPC controller is designed. First, Equation (6) is discretized with a sampling time of Ts = 0.01 s, yielding:

$$x(k+1) = Ax(k) + B_u u(k) + B_d \widetilde{d}(k) \tag{7}$$

where $A = e^{A_c T_s}$, $B_u = \int_0^{T_s} e^{A_c \tau} B_{u,c} \mathrm{d}\tau$, and $B_d = \int_0^{T_s} e^{A_c \tau} B_{d,c} \mathrm{d}\tau$ are the discretized system matrices. Considering that the measured disturbance signals vary relatively little within a short prediction horizon, the current measured value is extrapolated during the prediction process, i.e., the disturbance is approximately regarded as a constant value over the prediction horizon.

The controller takes the vertical, pitch, and roll accelerations of the cab as the optimization outputs. Since the outputs are not only related to the system states but also affected by the current control inputs and disturbances, the output equation can be expressed as:

$$\mathrm{y}(k) = Cx(k) + D_u u(k) + D_d \widetilde{d}(k) \tag{8}$$

where $y = \left[\ddot{z}_c, \ddot{\theta}_c, \ddot{\varphi}_c\right]^{\mathrm{T}} = \ddot{q}_c$ is the output vector, $C = \left[-M_c^{-1}K_c \quad -M_c^{-1}C_c\right]$, $D_u = M_c^{-1}B_u$, and $D_d = M_c^{-1}\left[B_d \quad C_d\right]$. The prediction horizon $N_p = 20$ and the control horizon $N_c = 10$ are selected, and the performance index is constructed as:

$$\begin{aligned} \min_{u(k|k),\ldots,u(k+N_c-1|k)} J(k) = & \sum_{j=1}^{N_p} \|y(k+j|k)\|_Q^2 \\ & + \sum_{j=0}^{N_c-1} \|u(k+j|k)\|_R^2 \\ & + \sum_{j=0}^{N_c-1} \|\Delta u(k+j|k)\|_S^2 \end{aligned} \tag{9}$$

where $Q = \mathrm{diag}\left(q_z, q_\theta, q_\varphi\right)$ is the output weighting matrix. Under the braking condition, greater emphasis is placed on pitch suppression, with $q_z = 1.0$, $q_\theta = 1.2$, and $q_\varphi = 0.6$. Under the steering condition, greater emphasis is placed on roll suppression, with $q_z = 1.0$, $q_\theta = 0.6$, and $q_\varphi = 1.2$. $R = 10^{-6} I_4$ and $S = 10^{-4} I_4$ are the weighting matrices for the desired controllable damper force and control increment, respectively, which are used to adjust the magnitude and variation rate of the control action.

The optimization objective considers not only the vibration responses of the cab but also the control effort required by the semi-active suspension. Therefore, the proposed MPC controller simultaneously minimizes the vertical, pitch, and roll accelerations while

avoiding excessive damper force variation. This formulation enables coordinated regulation of cab vibration and attitude responses under transient operating conditions.

The constraint conditions include:

$$\begin{aligned} -2000\ \text{N} \le u_i(k+j|k) \le 2000\ \text{N} \\ -200\ \text{N} \le \Delta u_i(k+j|k) \le 200\ \text{N} \end{aligned} \tag{10}$$

where $\Delta u_i(k+j \mid k) = u_i(k+j \mid k) - u_i(k+j-1 \mid k)$ represents the control increment. This optimization problem is formulated as a quadratic programming problem, which can be solved online at each sampling instant. The first control input of the optimal control sequence is applied to the system. These constraints are introduced to ensure that the commanded controllable damper forces and their increments remain within the physical operating range of the CDC dampers, thereby improving the practical feasibility of the proposed semi-active control strategy.

The main MPC parameters used in this study, including the prediction horizon, control horizon, weighting matrices, and actuator constraints, are determined according to the control objectives and physical limitations of the CDC dampers. These parameters are kept identical for the same operating condition during all simulations to ensure a consistent comparison between the passive and MPC-controlled suspensions.

The MPC weighting strategy in Equation (9) reflects a condition-dependent trade-off among vertical ride comfort, cab pitch and roll regulation, and control effort, rather than independently minimizing a single response. Under braking conditions, a larger relative weight is assigned to pitch suppression because longitudinal deceleration primarily excites the cab pitch response. Under steering conditions, a higher weight is assigned to roll suppression because lateral excitation induces a more pronounced cab roll response. Meanwhile, vertical acceleration remains included in the optimization objective under both conditions to maintain the overall ride comfort performance. In addition, the weighting matrices R and S penalize the magnitude and variation in the controllable damper forces, respectively, while the constraints in Equation (10) bound the controllable damper forces and their increments within feasible operating limits. Therefore, the proposed MPC strategy achieves a condition-dependent compromise among the coupled vertical, pitch, and roll responses while maintaining feasible semi-active control actions.

4.3. MPC Model Based on Measured Disturbances

To achieve attitude control simulation of the commercial vehicle cab under emergency braking and steering conditions, an MPC model incorporating measured disturbance information was established based on the MATLAB/Simulink R2024b platform. Unlike traditional methods that generate or estimate system disturbances through road surface models, this study utilizes the vertical acceleration signals at the lower ends of the suspensions collected from real vehicle road tests. The corresponding displacement time signals are obtained through filtering and integration processing and are used as known feedforward disturbance inputs, thereby improving the consistency between the disturbance inputs and the actual vehicle operating conditions.

Figure 10 illustrates the structure of the MPC system based on measured disturbances. After preprocessing, the measured disturbance signals are input into the MPC controller. The controller combines the current cab state information, solves the optimization problem online, and outputs the desired controllable damper force commands to the four semi-active suspension actuators.

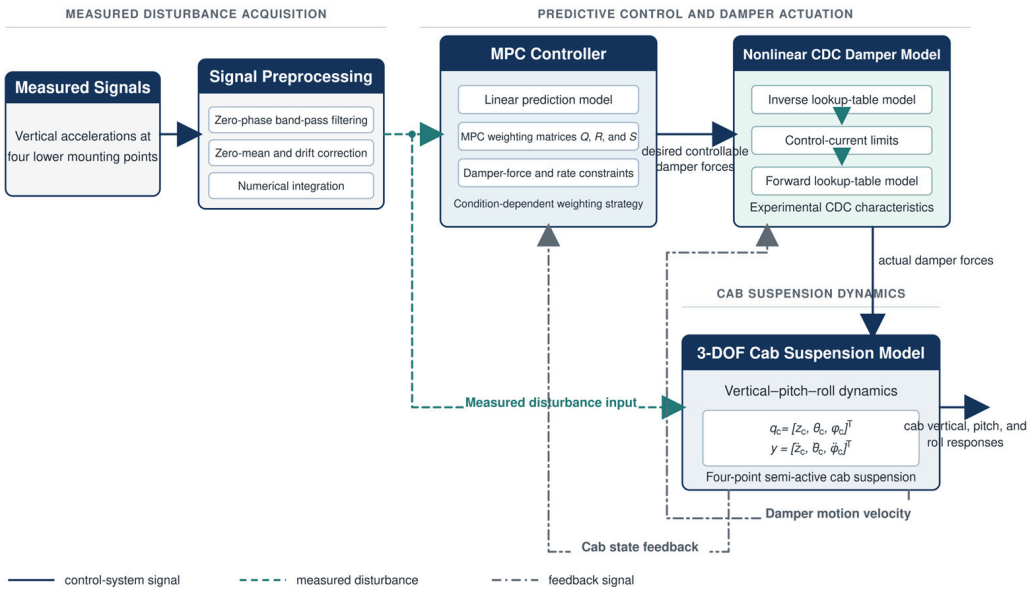

Figure 10. Block diagram of the MPC system based on measured disturbances.

5. Simulation Evaluation and Result Comparison

5.1. Evaluation Method of Cab Vibration Response

The control performance is evaluated using three complementary indicators. The RMS value is used to quantify the overall vibration level during the transient maneuver, while the peak response reflects the maximum instantaneous attitude disturbance experienced by the cab. Furthermore, the proposed weighted comprehensive index is introduced to evaluate the overall coordinated improvement of vertical, pitch, and roll responses under the same operating condition, while simultaneously highlighting the optimization of the dominant attitude response associated with each specific maneuver through condition-dependent weighting coefficients.

To comprehensively evaluate the relative contributions of the vertical, pitch, and roll responses to cab attitude control under the investigated transient conditions, a three-directional weighted comprehensive index is defined in this study. The multiplying factors for rotational vibration are adopted with reference to ISO 2631-1:1997. Specifically, the factors 0.63 m/rad and 0.4 m/rad are used for roll and pitch rotational vibration, respectively, so that the corresponding angular acceleration responses can be converted into quantities dimensionally consistent with vertical acceleration. It should be emphasized that the proposed index is an author-defined condition-oriented comparative metric rather than the standard vibration total value prescribed by ISO 2631-1. It is used only to compare the relative multi-directional response performance of the passive and MPC-controlled cab suspensions under the same transient operating condition, rather than to determine an absolute ride comfort level. The calculation formula is as follows:

$$RMS_{weighted} = w_x \cdot 0.63 \cdot RMS_x + w_y \cdot 0.4 \cdot RMS_y + w_z \cdot RMS_z \quad (11)$$

where RMS_x, RMS_y, and RMS_z represent the root mean square (RMS) values of the roll angular acceleration, pitch angular acceleration, and vertical acceleration at the cab center of gravity, respectively. The units of RMS_x and RMS_y are rad/s^2, whereas that of RMS_z is m/s^2. Therefore, multiplying RMS_x and RMS_y by 0.63 m/rad and 0.4 m/rad, respectively, converts the angular acceleration terms into quantities with the unit of m/s^2. Consequently, all three terms in Equation (11) are dimensionally consistent, and the resulting weighted index also has the unit of m/s^2.

The coefficients w_x, w_y, and w_z are dimensionless condition-dependent weighting coefficients corresponding to the relative importance assigned to the roll, pitch, and vertical responses, respectively. Their values are consistent with the relative output priorities adopted in the MPC objective function in Section 4.2. These evaluation weighting coefficients are used exclusively in the post-simulation calculation of Equation (11) and are distinct from the MPC output-weighting factors q_z, q_θ, and q_φ in the matrix Q. Although they reflect the same condition-dependent response priorities, they do not enter the MPC optimization. To clarify this correspondence, the numerical values of the MPC output-weighting factors and the evaluation weighting coefficients under the two operating conditions are summarized in Table 2.

Table 2. Correspondence between the MPC output-weighting factors and the evaluation weighting coefficients under braking and steering conditions.

Condition	w_x, Roll	w_y, Pitch	w_z, Vertical	MPC Matrix Q = diag(q_z,q_θ,q_φ)
Braking	0.6	1.2	1.0	$\mathrm{diag}(1.0, 1.2, 0.6)$
Steering	1.2	0.6	1.0	$\mathrm{diag}(1.0, 0.6, 1.2)$

The evaluation weighting coefficients correspond to w_x for roll, w_y for pitch, and w_z for vertical motion. Accordingly, (w_x, w_y, w_z) = (0.6, 1.2, 1.0) for braking and (1.2, 0.6, 1.0) for steering. Thus, the proposed index is used to evaluate whether the MPC-controlled suspension improves the dominant attitude response while simultaneously accounting for the contributions of the other two response directions.

Unlike the root-sum-of-squares combination used in ISO 2631-1 for standardized whole-body vibration assessment, a linear weighted summation is adopted in the present study because the purpose of Equation (11) is to provide a condition-oriented relative comparison rather than an absolute human comfort assessment. This linear form allows the contribution of each response direction to the overall evaluation result to be explicitly adjusted according to the dominant attitude characteristic of the investigated maneuver.

5.2. Simulation Under Emergency Braking Conditions

According to the aforementioned three-directional weighted comprehensive index, and considering the characteristics of the responses in different directions under braking conditions, the evaluation weighting coefficients of the vertical, pitch, and roll directions are set to 1.0, 1.2, and 0.6, respectively, for the emergency braking condition. These coefficients are used to quantitatively evaluate the improvement effect of MPC on cab vertical, pitch, and roll responses.

After the simulation, the vertical acceleration, pitch angular acceleration, and roll angular acceleration responses at the cab center of gravity under the MPC-controlled semi-active suspension system are compared with the corresponding responses of the passive suspension system. Meanwhile, the variations in the damper forces of the four semi-active suspensions during the simulation are analyzed to verify the rationality of their values and variation trends. The cab attitude control performance and damper force feasibility of the MPC controller are comprehensively evaluated under the emergency braking condition. The simulation results of the cab time-domain responses under the 20 km/h emergency braking condition are shown in Figure 11, and the calculation and comparison results of the four evaluation indicators are presented in Table 3.

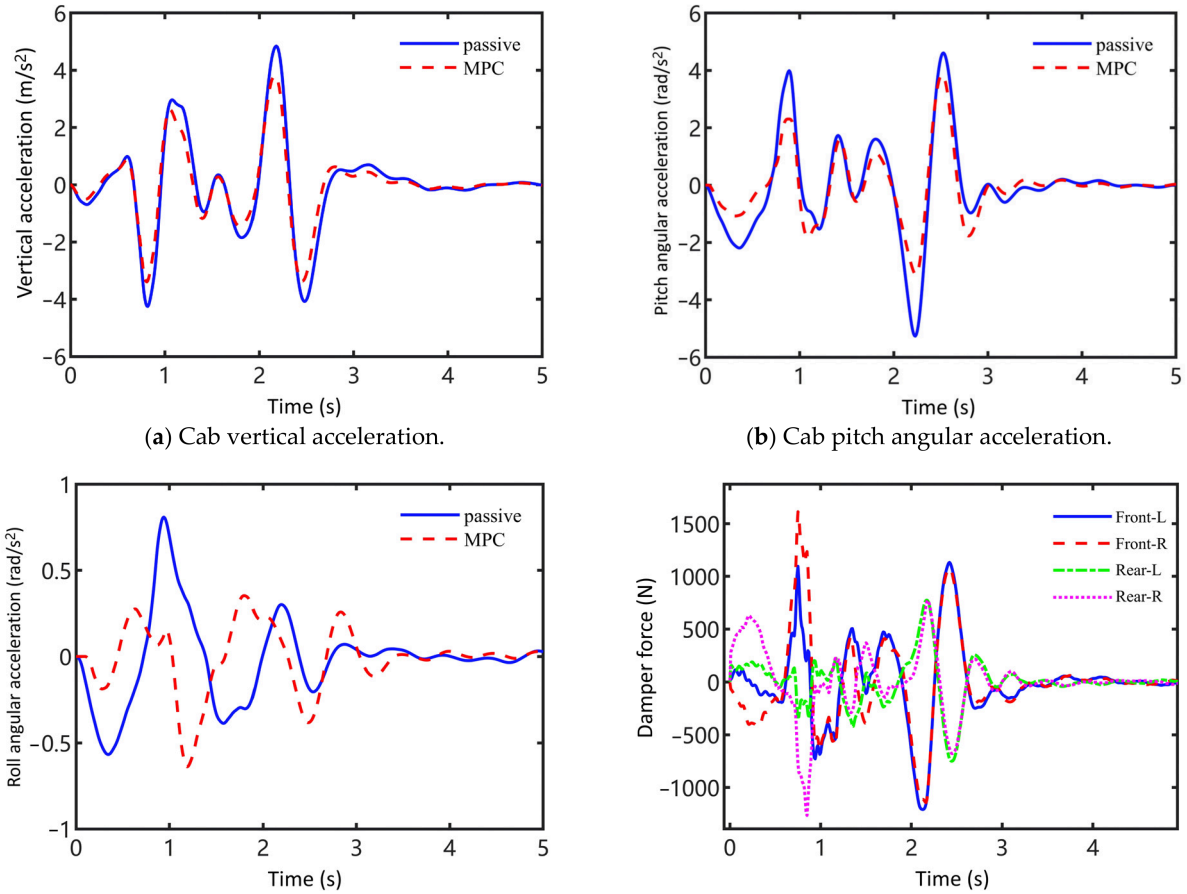

(**a**) Cab vertical acceleration.

(**b**) Cab pitch angular acceleration.

(**c**) Cab roll angular acceleration.

(**d**) Damper forces at the four cab-suspension mounts.

Figure 11. Time-domain responses of the cab under the 20 km/h emergency braking condition.

Table 3. Comparison of Cab Dynamic Response Evaluation Indicators under Braking Condition.

Evaluation Indicator	20 km/h Passive	20 km/h MPC (Improvement Rate)
RMS of vertical acceleration (m/s^2)	1.5576	1.2384 (−20.5%)
RMS of pitch angular acceleration (rad/s^2)	1.5846	1.1336 (−28.5%)
RMS of roll angular acceleration (rad/s^2)	0.2470	0.1893 (−23.4%)
Three-directional weighted comprehensive index	2.4116	1.8541 (−23.1%)

Compared with the passive suspension system, the semi-active suspension system controlled by the proposed MPC method achieves consistent improvements in all evaluated vibration and attitude-related metrics under the 20 km/h emergency braking condition. Specifically, the RMS value of the cab vertical acceleration is reduced by 20.5%, the RMS value of the pitch angular acceleration is reduced by 28.5%, the RMS value of the roll angular acceleration is reduced by 23.4%, and the three-directional weighted comprehensive index is reduced by 23.1%. These reductions indicate that the proposed controller effectively suppresses both overall vibration energy and attitude-related responses under the same transient excitation condition.

Given the deterministic and transient nature of the braking and steering maneuvers investigated in this study, the present analysis was not designed to include repeated-sample statistical significance testing. Therefore, the effectiveness of the proposed controller is evaluated based on consistent reductions in multiple engineering performance indicators, including RMS values, peak responses, and the weighted comprehensive index, under identical excitation inputs and operating conditions.

Further analysis of the simulation results shows that, in terms of vertical vibration, the cab experiences a large vertical acceleration at the initial stage of braking, followed by a decaying oscillation. The maximum vertical acceleration occurs at approximately 2.2 s, with a value of 4.8 m/s^2. As shown in Figure 11a, under the MPC proposed in this study, the energy of the cab vertical vibration is effectively reduced.

Regarding the pitch motion, as shown in Figure 11d, at the initial stage of braking, the front suspensions are compressed and generate a relatively large damper force to suppress the forward pitching motion of the vehicle body, while the rear suspensions are stretched and generate damper forces in the opposite direction. Together, they form a reverse moment that suppresses pitch motion. As shown in Figure 11b, under the 20 km/h condition, the passive suspension system reaches a maximum positive value of approximately 4.0 rad/s^2 at around 0.8 s. Within less than 0.2 s after this point, the MPC controller generates a controllable damper force distribution that generates an opposing pitch moment, reducing the maximum value to approximately 2.2 rad/s^2.

Regarding the roll motion, it can be observed from Figure 11c that the roll angular acceleration of the cab is relatively small under the braking condition. Although the contribution of roll motion is relatively limited under emergency braking, the MPC controller still reduces the corresponding RMS value. The transient roll response exhibits some phase differences compared with the passive suspension, which is attributed to the coordinated optimization of multiple coupled cab responses rather than independent roll suppression.

According to the three-directional weighted comprehensive index evaluation of the entire braking process, the MPC method demonstrates good vibration suppression performance. The vertical and pitch responses have a greater influence on the three-directional weighted comprehensive index, while the roll response is relatively small but is also reduced to some extent. This indicates that while the controller mainly focuses on the vertical and pitch attitude control of the cab, it also provides a certain degree of suppression for lateral vibration.

Considering the coordinated optimization of the front and rear suspension damper forces and the predictive pitch regulation capability, the proposed MPC strategy achieves noticeable improvements in peak reduction, vibration attenuation, and response regulation. These improvements are practically meaningful because reducing the transient pitch response during emergency braking can alleviate cab nose-diving behavior and improve driver visual stability, while the simultaneous reduction in vertical vibration contributes to improved ride comfort.

5.3. Simulation Under Steering Conditions

Similar to the emergency braking condition, according to the aforementioned three-directional weighted comprehensive index and the characteristics of responses in different directions under steering conditions, the evaluation weighting coefficients for the three-directional weighted comprehensive index under the steering condition are set as 1.0 for the vertical direction, 0.6 for the pitch direction, and 1.2 for the roll direction. These coefficients are used to quantitatively evaluate the control performance of the MPC strategy under the steering condition.

The simulation results are shown in Figure 12, and the comparison results of the four evaluation indicators are presented in Table 4.

To present the complete transient evolution under the steering condition, the response time histories in Figure 12a–d were extended to 10 s. The interval from 0 to 5 s contains the principal transient response induced by the steering maneuver, whereas the interval from 5 to 10 s is included to show the post-maneuver decay of the cab motion after the main disturbance has subsided. During this latter interval, the vertical, pitch, and roll responses

of both the passive and MPC-controlled cab suspensions progressively attenuate toward the equilibrium state, with only small residual oscillations remaining. The quantitative indicators for the steering condition are still calculated over the effective response interval of 0–5 s to maintain consistency in evaluating the principal transient response. For the braking condition, the original time history plots already capture both the principal response and its subsequent attenuation; therefore, their displayed time ranges were retained.

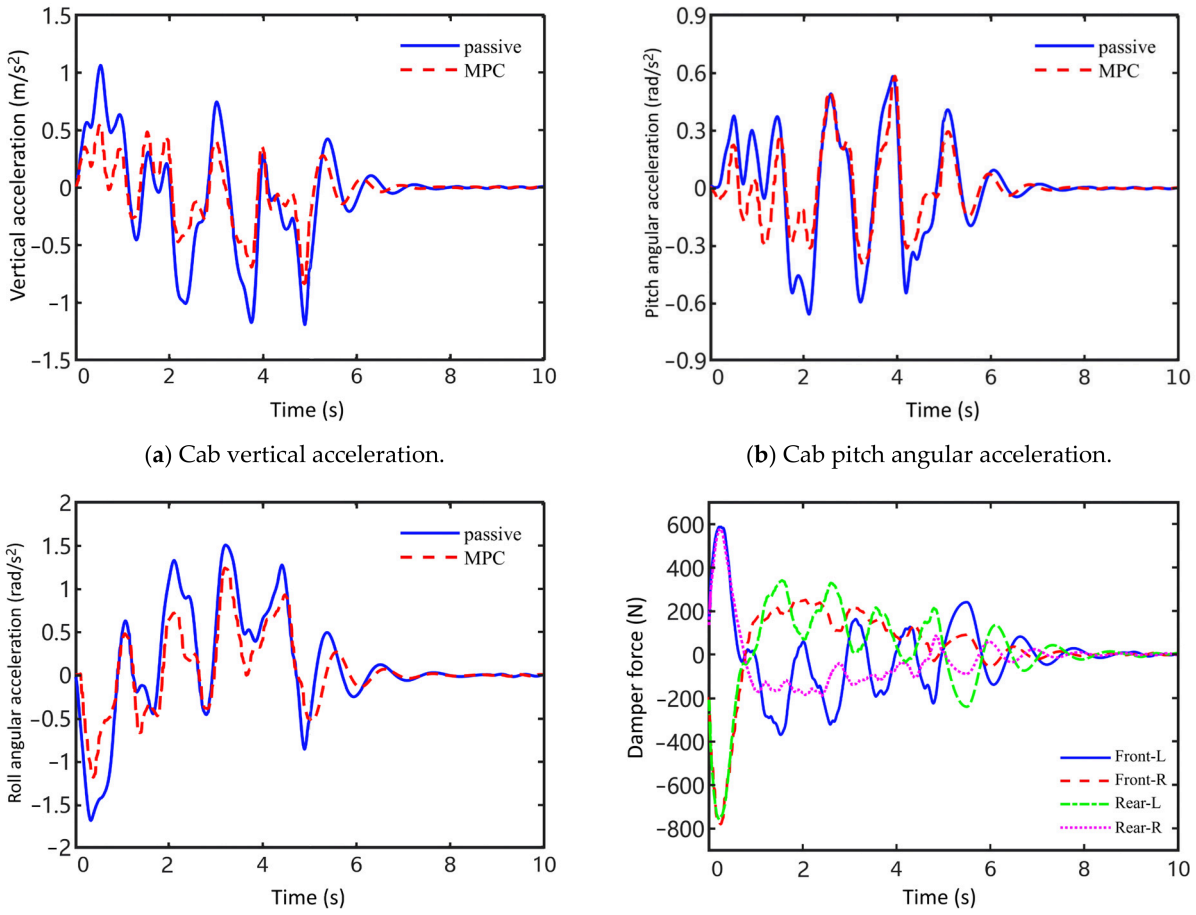

(**a**) Cab vertical acceleration.

(**b**) Cab pitch angular acceleration.

(**c**) Cab roll angular acceleration.

(**d**) Damper forces at the four cab suspension mounts.

Figure 12. Time-domain responses of the cab under the 25 km/h right-angle steering condition.

Table 4. Comparison of Cab Vertical, Pitch, and Roll Dynamic Responses under Steering Condition during 0–5 s.

Evaluation Indicator	25 km/h Passive	25 km/h MPC (Improvement Rate)
RMS of vertical acceleration (m/s^2)	0.5717	0.4287 (−24.9%)
RMS of pitch angular acceleration (rad/s^2)	0.3369	0.2872 (−14.8%)
RMS of roll angular acceleration (rad/s^2)	0.8602	0.5670 (−34.1%)
Three-directional weighted comprehensive index	1.3029	0.9263 (−28.9%)

Figure 12a presents the time history of the cab vertical acceleration under the 25 km/h steering condition. It can be observed that after applying MPC, the vertical vibration amplitude is significantly reduced, the fluctuation range is decreased, and the oscillations decay

more rapidly. As shown in Table 4, the RMS value of the vertical acceleration decreases from 0.5717 m/s^2 to 0.4287 m/s^2, corresponding to a reduction of 24.9%. Figure 12b shows the variation in the pitch angular acceleration. Under the 25 km/h steering condition, the pitch angular acceleration changes slightly, and no obvious impact response occurs. After applying MPC, the RMS value of the pitch angular acceleration decreases from 0.3369 rad/s^2 to 0.2872 rad/s^2, with a reduction rate of 14.8%. Roll motion is an important aspect of cab attitude control under steering conditions. As shown in the comparison of roll angular acceleration in Figure 12c, the passive suspension system exhibits a relatively large roll response with significant variations. After applying the MPC method, the RMS roll angular acceleration is substantially reduced. Its RMS value decreases from 0.8602 rad/s^2 to 0.5670 rad/s^2, representing a reduction of 34.1%, which is the best improvement among the three directions. The reduction in roll response is particularly meaningful for commercial vehicles because lateral load transfer during steering maneuvers can directly influence cab attitude stability and driver perception. Therefore, the improvement in roll suppression demonstrates the practical benefit of the proposed MPC strategy in mitigating steering-induced attitude deviation. In addition, according to the three-directional weighted comprehensive index, the overall improvement of MPC under the steering condition is 28.9%, indicating that the comprehensive cab attitude control capability is significantly improved.

Roll control mainly relies on the asymmetric coordinated output of the damper forces of the left and right suspensions. As shown in Figure 12d, during the initial steering stage from 0 to 1 s and the period from 2 to 3 s, the MPC controller coordinates the different damper forces of the front-left, front-right, rear-left, and rear-right suspensions, resulting in a significant reduction in the peak values of roll angular acceleration. The results indicate that under steering conditions, MPC can continuously suppress roll motion by regulating the different controllable damper force outputs of the left and right suspensions, while retaining coordinated regulation of the vertical and pitch responses. The response curve becomes smoother, and the oscillations decay faster. Furthermore, the optimization of roll control also improves the vertical response, forming an attitude control system dominated by roll control with multi-directional coordinated operation, thereby enhancing the cab attitude control capability under steering conditions.

This result also demonstrates the condition-dependent trade-off implemented by the MPC strategy: although roll suppression is given higher priority during steering, the vertical and pitch responses remain included in the optimization objective, allowing improved roll regulation without neglecting the other cab motion responses.

6. Conclusions

This study investigates the attitude control problem of a commercial vehicle cab suspension system under braking and steering conditions. First, road sampling tests were conducted to collect the measured acceleration signals at the lower ends of the four suspension points under braking and steering conditions. The collected signals were then converted into displacement signals through filtering and integration processing, which were used as feedforward disturbance inputs to characterize the actual excitations filtered by the chassis system. Second, performance tests of the CDC dampers were carried out, and the damper model and cab dynamic model were established. The MPC prediction model was constructed after linearization. It should be noted that the linear prediction model adopted in the present study is intended for the specific transient operating range investigated here, namely the 20 km/h emergency braking maneuver and the 25 km/h right-angle-steering maneuver. The model is not intended to reproduce all nonlinear characteristics of the complete vehicle under extreme handling conditions. Its primary purpose is to capture the dominant vertical, pitch, and roll dynamics required for real-

time predictive control, while the experimentally identified nonlinear characteristics of the CDC dampers are retained separately in the actuator model. For maneuvers involving large suspension deflections, large cab attitude angles, or operating conditions outside the experimentally characterized damper range, nonlinear prediction models may provide higher prediction accuracy and will be considered in future work. Furthermore, a discrete-time MPC controller was designed based on the state-space model. The objective of the controller is to optimize the vertical, pitch, and roll accelerations of the cab and achieve cab attitude control under braking and steering conditions. The MPC prediction explicitly accounts for the effects of the current control input and the measured disturbance, in addition to the cab motion states, on the predicted outputs.

To evaluate the attitude control performance of the MPC-based commercial vehicle cab, a three-directional weighted comprehensive index was established based on the vertical, pitch, and roll responses at the cab center of gravity to evaluate the influence of multi-directional vibrations on cab attitude stability. Simulations of the 20 km/h emergency braking condition and the 25 km/h steering condition were carried out using the MATLAB/Simulink platform. The simulation results show that, compared with the conventional suspension system, under the 20 km/h emergency braking condition, the three-directional weighted comprehensive index is reduced by 23.1%, and the pitch angular acceleration is reduced by 28.5%. Under the 25 km/h steering condition, the three-directional weighted comprehensive index is reduced by 28.9%, and the roll angular acceleration is reduced by 34.1%. The simulation results demonstrate that, under the proposed MPC method, the semi-active cab suspension system of the commercial vehicle achieves significant improvements in the vertical, pitch, and roll responses as well as the three-directional weighted comprehensive index. The effectiveness of the MPC method in improving the cab attitude control capability of the investigated commercial vehicle is verified.

Although the disturbance inputs used in this study were obtained from real-vehicle road tests and the CDC damper model was established based on experimental characterization, the proposed MPC controller was evaluated at the simulation level. Therefore, the present results should be interpreted as simulation-based verification under experimentally measured disturbances rather than full experimental validation of the closed-loop control system. Future work will focus on hardware-in-the-loop, suspension-bench, and full-vehicle implementation to further evaluate real-time computational performance, actuator delay, measurement uncertainty, and model mismatch.

Author Contributions: Conceptualization, Y.J. and C.Y.; methodology, Z.A. and Y.L.; software, Z.A.; validation, Y.J., J.L. and L.L.; formal analysis, Y.J. and L.L.; investigation, J.L.; resources, C.Y.; data curation, Z.A.; writing—original draft preparation, Y.J.; writing—review and editing, Z.A.; visualization, Y.L.; supervision, L.L.; project administration, J.L.; funding acquisition, C.Y. All authors have read and agreed to the published version of the manuscript.

Funding: This research was supported by the Hubei Provincial Science and Technology Innovation Base (Platform) Program under Grant number 2024CSA082 and Hubei Province Technology Innovation Program under Grant number 2026BAB117.

Informed Consent Statement: Informed consent for participation was obtained from both the driver and the test engineer involved in the road tests.

Data Availability Statement: The data that support the findings of this study are available from the corresponding author, Changcheng Yin, upon reasonable request.

Conflicts of Interest: Author Liang Li was employed by the company Engineering Validation Center, Product R&D Institute, Dongfeng Motor Group (China). Author Jun Liu was employed by the company Product Service Center, Xiangyang DAAN Automobile Test Center Co., Ltd. The remaining

authors declare that the research was conducted in the absence of any commercial or financial relationships that could be construed as a potential conflict of interest.

References

1. Lu, Y.; Wang, T.; Zhang, H. Multiobjective Synchronous Control of Heavy-Duty Vehicles Based on Longitudinal and Lateral Coupling Dynamics. *Shock Vib.* **2022**, *2022*, 6987474. [CrossRef]
2. Yin, Z.H.; Liang, Z.M.; Luo, J.; Shangguan, W.F.; Li, B. Pitch Motion Control of Vehicles Based on Fully Active Suspension. *J. South China Univ. Technol. (Nat. Sci. Ed.)* **2026**, *54*, 1–11. [CrossRef]
3. Metered, H.; Ibrahim, I.M. Vibration Mitigation of Commercial Vehicle Active Tandem Axle Suspension System. *SAE Int. J. Commer. Veh.* **2022**, *15*, 275–287. [CrossRef]
4. Gong, M.; Chen, H.; Zhao, D.; Zhu, J.-X.; Deng, Y.-J.; Song, H.-X. Active Suspension Control Strategy of Heavy Rescue Vehicle Based on Multi-Sensor Information Fusion. *Proc. Inst. Mech. Eng. Part D J. Automob. Eng.* **2023**, *237*, 1338–1352. [CrossRef]
5. Xu, H.; Chen, Z.; Wu, D.; Feng, J.; Xu, G.; Ning, Z.-X. Research on Road Tracking and Anti-Roll Game Control Scheme of Commercial Vehicle Based on Nash Equilibrium. *Proc. Inst. Mech. Eng. Part D J. Automob. Eng.* **2024**, *238*, 3160–3171. [CrossRef]
6. Pang, L.; Yue, M.; Qi, G.; Zhao, X. Switched Control Strategy Based on Preview-Based MPC for Active Suspension of Heavy-Duty Vehicle to Improve Ride Comfort and Roll Stability. *Meas. Sci. Technol.* **2025**, *36*, 036201. [CrossRef]
7. Ma, C.; Hu, Y.; Zhao, W.; Zeng, D. Mix Controller Design for Active Suspension of Trucks Integrated with Online Estimation of Vehicle Mass. *Vehicles* **2025**, *7*, 71. [CrossRef]
8. Do, T.T. Enhanced Vehicle Dynamics through Constrained Model Predictive Control for In-Wheel Active Suspension Systems. *Proc. Eng. Technol. Innov.* **2026**, *32*, 73–84. [CrossRef]
9. Zhao, H.L. Research on Semi-Active Suspension Mount Control Method for Ride Comfort and Handling Stability. Master's Thesis, Guilin University of Electronic Technology, Guilin, China, 2024. [CrossRef]
10. Liu, H.; Liu, X.; Wei, A.; Cai, Y. Dynamic Response Analysis of Asphalt Pavement under Pavement-Unevenness Excitation. *Appl. Sci.* **2024**, *14*, 8822. [CrossRef]
11. Yin, Z.; Cui, C.; Wang, R.; Su, R.; Ma, X. Improving Vehicle Dynamics: A Fractional-Order PIλDμ Control Approach to Active Suspension Systems. *Machines* **2025**, *13*, 271. [CrossRef]
12. Li, K.T. Research on Electronic Air Suspension Control Under Straight Uniform Speed and Emergency Braking Conditions. Master's Thesis, Jiangsu University of Science and Technology, Zhenjiang, China, 2022. [CrossRef]
13. Wang, L.F. Research on Safety and Comfort Control Strategy of Passenger Cars Under Braking Conditions. Master's Thesis, Jilin University, Changchun, China, 2024. [CrossRef]
14. Zhao, H.L.; Liu, H.Q.; Liu, F.Y.; Deng, J.C.; Li, D.; Zhang, X. Semi-active suspension control strategy for commercial vehicle cab pitch vibration. *Sci. Technol. Eng.* **2024**, *24*, 8306–8313. [CrossRef]
15. Liu, J.Y. Research on Handling Stability Optimization Control of Commercial Vehicles Using Semi-Active Suspension. Master's Thesis, Jilin University, Changchun, China, 2024. [CrossRef]
16. Kang, S.Y. Research on Vehicle Attitude Coordination Control Based on the Damping Characteristics of Semi-Active Suspension Dampers. Master's Thesis, Taiyuan University of Technology, Taiyuan, China, 2024. [CrossRef]
17. Yao, J.L.; Wang, S.; Chen, A.L.; Tian, J.; Wang, Z.; Guo, L.-X. Semi-active actuator-based hybrid model predictive control for vehicle tilting. *Proc. Inst. Mech. Eng. Part D J. Automob. Eng.* **2025**, *240*, 2886–2896. [CrossRef]
18. *GB/T 4970-2009*; Method of Running Test—Automotive Ride Comfort. China Standards Press: Beijing, China, 2009.
19. *ISO 2631-1:1997*; Mechanical Vibration and Shock-Evaluation of Human Exposure to Whole-Body Vibration-Part 1: General Requirements. International Organization for Standardization: Geneva, Switzerland, 1997.
20. Liu, F.; Gao, S.; Chang, S. Displacement estimation from measured acceleration for fixed offshore structures. *Appl. Ocean Res.* **2021**, *113*, 102741. [CrossRef]
21. Ursel, T.W.; Olinski, M. Displacement Estimation Based on Optical and Inertial Sensor Fusion. *Sensors* **2021**, *21*, 1390. [CrossRef] [PubMed]
22. Zhang, X.; Liu, F.Y.; Deng, J.C.; Chen, Z.; Wang, Y.; Li, D. A discrete signal numerical integration method for semi-active suspension and its application. *Noise Vib. Control* **2023**, *43*, 166–172. [CrossRef]
23. Paik, S.; Raghuvanshi, J.; Chaudhari, V.V.; Radhika, V. Assessment of low-frequency structure-borne road noise for battery electric vehicle: Prediction and improvement. In *Proceedings of the Symposium on International Automotive Technology, Pune, India, 28 January 2026*; SAE Technical Papers on CD-ROM/SAE Technical Paper Series; SAE International: Warrendale, PA, USA, 2026. [CrossRef]
24. Kurbanov, S.V.; Andrikov, D.A.; Agasieva, S.V.; Iaroshenko, A.V. Digital Modelling of Low-Frequency ECG Signals Denoising. *RUDN J. Eng. Res.* **2025**, *26*, 447–456. [CrossRef]
25. Walters, S.J.; Turner, R.; Forbes, L.K. A comparison of explicit Runge-Kutta methods. *ANZIAM J.* **2023**, *64*, 227–249. [CrossRef]

26. Chintala, P.; Patwa, A.; Sankaran, S. Design and Development of Base Valve for a Semi-Active Damper. In *Proceedings of the WCX SAE World Congress Experience, Detroit, MI, USA, 16 April 2024*; SAE Technical Papers on CD-ROM/SAE Technical Paper Series; SAE International: Warrendale, PA, USA, 2024. [CrossRef]
27. *QC/T 491-2018*; Automobile Shock Absorber Technique Requirements and Test Methods. China Communications Press: Beijing, China, 2018.
28. Du, C.; Yin, Z.; Xia, Z.; Wang, W.; Shangguan, W.-B. Control Strategy for Semi-Active Suspension Based on Suspension Parameter Estimation. In *Proceedings of the WCX SAE World Congress Experience, Detroit, MI, USA, 16 April 2024*; SAE Technical Papers on CD-ROM/SAE Technical Paper Series; SAE International: Warrendale, PA, USA, 2024. [CrossRef]
29. Ji, G.; Li, S.; Feng, G.; Li, Z.; Liu, X. A novel DNFS control strategy for vehicle semi-active suspension system. *Meas. Sci. Technol.* **2024**, *35*, 126203. [CrossRef]
30. Jiao, H.; Shu, R.; Zeng, Z.; Tang, X.; Shu, H. Explicit Solution for Improvement of Real-time Performance of Model Predictive Control in Intelligent Vehicle Stability. *J. Mech. Eng.* **2025**, *61*, 263–275. [CrossRef]
31. Magalhães, Z.; Murilo, A.; Lopes, R.V. Vehicle Stability Upper-Level-Controller Based on Parameterized Model Predictive Control. *IEEE Access* **2022**, *10*, 21048–21065. [CrossRef]
32. Zhang, J.; Yang, Y.; Hu, M.; Fu, C.; Zhai, J. Model Predictive Control of Active Suspension for an Electric Vehicle Considering Influence of Braking Intensity. *Appl. Sci.* **2021**, *11*, 52. [CrossRef]
33. Hegedűs, T.; Németh, B.; Gáspár, P. MPC Based Semi-active Suspension Control for Overtaking Maneuvers. *Period. Polytech. Transp. Eng.* **2021**, *49*, 224–230. [CrossRef]
34. Xu, T.; Hu, J.; Sun, G.; Wen, J.; Chen, D.; Huang, Y.; Zhang, P. Roll–Vertical Coupled Roll State Estimation and Coordinated Control for Active Suspension Vehicles. *Mathematics* **2026**, *14*, 2881. [CrossRef]

Disclaimer/Publisher's Note: The statements, opinions and data contained in all publications are solely those of the individual author(s) and contributor(s) and not of MDPI and/or the editor(s). MDPI and/or the editor(s) disclaim responsibility for any injury to people or property resulting from any ideas, methods, instructions or products referred to in the content.